Helmholtz-Zentrum
Geesthacht
Zentrum für Material- und Küstenforschung

Final Draft
of the original manuscript:

Yi, X.; Huenicke, B.; Tim, N.; Zorita, E.:

The relationship between Arabian Sea upwelling and Indian Monsoon revisited in a high resolution ocean simulation

In: Climate Dynamics (2017) Springer

DOI: 10.1007/s00382-017-3599-8

The relationship between Arabian Sea upwelling and Indian Monsoon revisited in a high resolution ocean simulation

Xing Yi, Birgit Hünicke, Nele Tim and Eduardo Zorita

Helmholtz-Zentrum Geesthacht, Institute of Coastal Research, Max-Planck-Str.1, Geesthacht, 21502, Germany

Correspondence to: Xing Yi (email: xing.yi@hzg.de; tel: +494152872821; fax: +494152872818)

Abstract

Studies based on sediment records, sea-surface temperature and wind suggest that upwelling along the western coast of Arabian Sea is strongly affected by the Indian summer Monsoon (ISM). We examine this relationship directly in an eddy-resolving global ocean simulation STORM driven by atmospheric reanalysis over the last 61 years. With its very high spatial resolution (10 km), STORM allows us to identify characteristics of the upwelling system. We analyse the co-variability between upwelling and meteorological and oceanic variables from 1950 to 2010. The analysis reveals high interannual correlations between coastal upwelling and along-shore wind-stress (r=0.73) as well as with sea-surface temperature (r=-0.83). However, the correlation between the upwelling and the ISM is small. We find an atmospheric circulation pattern different from the one that drives the Monsoon as the main modulator of the upwelling variability. In spite of this, the patterns of temperature anomalies that are either linked to Arabian Sea upwelling or to the Monsoon are spatially quite similar, although the physical mechanisms of these links are different. In addition, no long-term trend is detected in our modelled upwelling in the Arabian Sea.

Keywords

Arabian Sea upwelling; Indian summer Monsoon; high resolution ocean simulation

Acknowledgements

This work is funded by the Cluster of Excellence Integrated Climate System Analysis and Prediction (CliSAP) Project B3. We thank the Max-Planck-Institute for Meteorology for providing the model data. All the other publicly available data used in this study are gratefully acknowledged.

1. Introduction

Coastal upwelling is important for ocean primary production as the upwelled cold nutrient-rich water supports coastal fisheries. In the Arabian Sea, one of the most important coastal upwelling regions along with the Eastern Boundary Upwelling Systems (EBUSs), upwelling is mainly controlled by the along-shore wind-stress during the summer season. It has been generally assumed that the variations of upwelling-favourable winds in this region are connected to the variations of the Indian Monsoon (Findlater 1969). To understand the relationship between the Arabian Sea upwelling and the Indian Monsoon is of great importance. During the upwelling season, the Monsoon brings moisture from south in the Indian Ocean to the Indian subcontinent in the North and causes rainfall there, which is essential to the local population. Because the upwelling cools the ocean surface, an intensified (reduced) upwelling would weaken (enhance) the ocean surface evaporation leading to less (more) precipitation over the Indian subcontinent (Izumo et al. 2008). However, since there are little direct observations of ocean vertical velocity, it has been difficult to directly ascertain the link between the Arabian Sea upwelling and the Indian Monsoon. In this study, we revisit this connection by analysing a very high-resolution ocean simulation with the model MPI-OM driven by meteorological reanalysis over the last decades.

Additionally, it has been hypothesized that coastal upwelling will strengthen in the major upwelling regions under the influence of global warming (Bakun 1990). In support of this hypothesis, Narayan et al. (2010) detected positive trends in upwelling intensity in the four major EBUSs and more recently Wang et al. (2015) projected the intensification of upwelling in three of the four EBUSs under a strong increase of anthropogenic greenhouse gas emissions. In the Arabian Sea, although little is known about the upwelling trends in terms of vertical velocity over the last few decades, Liao et al. (2015) found that the sea surface temperature (SST) along the Indian Ocean (including the Arabian Sea) coast revealed a reversed trend between the global warming period (1982-1998) and the warming hiatus period (1998-2013), which is related to the focus of the present study due to the close relationship between upwelling and the coastal SST. Bakun's hypothesis is related to the intensification of the land-ocean temperature gradient due to an intensification of the anthropogenic greenhouse gas forcing. We will also analyse to what extent the results from this simulation indicate an intensification of upwelling in the Arabian Sea over the past decades are compatible with this hypothesis.

The Arabian Sea upwelling and its relationship with the Indian summer Monsoon (ISM) have been broadly investigated. Studies based on the abundance of the foraminiferan *G. bulloides* from the sediment records intimately connected the Arabian Sea upwelling and the ISM (Anderson et al. 2002; Curry et al. 1992; Kroon et al. 1991; Prell and van Campo 1986). Since upwelling advects colder water masses to the surface, sea-surface temperature (SST) is thought to be the most reliable indicator of the coastal upwelling in the Arabian Sea (Prell and Curry 1981) and it has been applied as a traditional upwelling index by various studies. More recently, Godad et al. (2011) reconstructed the SST from planktonic foraminifera and suggested that the peak upwelling season has shifted over the last 22,000 years in the western Arabian Sea. A comparison between the foraminifera collected from sediment traps in the western and the eastern Arabian Seas showed that the abundances were significantly correlated to the Monsoon but not to the SST and CO_2 (Naik et al. 2013). Emeis et al. (1995) used SST reconstructed from sediment records and Manghnani et al. (1998) processed SST from remote sensing data, while Izumo et al. (2008) combined modelled, in situ and satellite SST data, to derive an upwelling index. In addition, other previous studies have used along-shore upwelling favourable wind-stress as another traditional upwelling index, as originally described by Bakun (1973). Recently, Varela et al. (2015) reported a negative trend in the wind-stress along the Somalia-Oman coast from 1982 to 2010 and deCastro et al. (2016) projected a strengthened upwelling along the Somalia coast (very closely located to the Arabian Sea) in the future.

These upwelling indices have been profusely used but they are not a direct measure of upwelling velocities. It is difficult to monitor vertical velocities over a long time span and therefore other studies have resorted to ocean simulations to study changes in the vertical velocity during upwelling. Recently, Jacox et al. (2014) analysed the vertical velocity from a four-dimensional regional ocean model to investigate the upwelling in the California current system. In the Arabian Sea, Shi et al. (2000) estimated the upwelling velocity off Oman from 1993 to 1995 through the combination of hydrographic and altimetry data. Anderson et al. (1992) employed a simple one-dimensional model to calculate the vertical upwelling velocity off Oman. Rao et al. (2008) used a three-dimensional model to compute the vertical velocity along the west coast of India. Studies applying ocean general circulation models also gave hints on the interaction of upwelling and SST (Ma et al. 2014) and the impact of Kelvin waves at the eastern boundary on the western Arabian Sea upwelling region (Tozuka et al. 2014). However, in terms of modelling applications, a study focused on the western Arabian Sea based on long-term four dimensional upwelling data is not yet available. In this study we fill this gap by employing the direct upwelling velocity data modelled in a high-resolution global ocean simulation over the period 1950 to 2010. We compare the upwelling velocity with traditional upwelling indices (SST and wind-stress) and examine the relationship between the upwelling and the ISM as well as other potential factors that might affect the upwelling. An unexpected finding is that the correlations between the simulated upwelling and three different monsoon indices are low and insignificant, which indicates that over the past 61 years the impact of the ISM on the coastal upwelling in the western Arabian Sea could have been weaker than previously thought and that other large-scale atmospheric forcing is a more efficient driver of upwelling in this region.

2. Model and Data

The German consortium project STORM is aimed at developing high-resolution global climate change simulations. The ocean model simulation used in this study is hereinafter referred to as the STORM simulation, which is described in von Storch et al. (2012). It is based on the Max-Planck Institute Ocean Model (MPI-OM) and is forced by the 6 hourly National Centers for Environmental Prediction (NCEP) / National Center for Atmospheric Research (NCAR) reanalysis (Kalnay et al. 1996) for the period from 1948 to 2010. The model's original bipolar grid is replaced by a tripolar grid to obtain an isotropic horizontal resolution. Comprising 3602 × 2394 horizontal grid points in total, the STORM simulation has a horizontal resolution of 0.1° around the equator but coarser towards the poles. The model has 80 levels, separated in the first 200 m by 10 to 15 m.

Upwelling velocity is derived from the vertical water mass transport in the STORM simulation output. The high spatial resolution of the STORM simulation allows us to capture the upwelling variability on small scales. The chosen upwelling domain (Fig. 1) extends about 90 km offshore along the coast of Yemen and Oman between 15.2°N to 22.3°N (Rixen et al. 2000). According to Brock and McClain (1992), we average the upwelling velocity over the upper 200 m of water. We compare the upwelling velocity derived from the STORM simulation with observational SST and wind-stress derived from different sources. SST data are obtained from the Advanced Very High Resolution Radiometer (AVHRR) Pathfinder Version 5.0 (Casey et al. 2010). Wind data are provided by the NCEP/NCAR reanalysis and the Cross-Calibrated Multi-Platform (CCMP) project (Atlas et al. 2011). The area selected for calculation of the wind data time series is the entire ocean domain in Fig. 1. Since different wind datasets are applied and compared here, for the sake of consistency we calculate the wind-stress from the wind datasets instead of using directly the native wind-stress to avoid any bias between the algorithms used to derive the wind-stress by different projects. The along-shore upwelling favourable wind-stress is calculated as:

$$\boldsymbol{\tau_{SW}} = \boldsymbol{\rho} \cdot \boldsymbol{C_D} \cdot \sqrt{\boldsymbol{u}^2 + \boldsymbol{v}^2} \cdot (\boldsymbol{u} \cdot \boldsymbol{cos\alpha} + \boldsymbol{v} \cdot \boldsymbol{cos\beta})$$

where $\boldsymbol{\rho}$ is the air density which is assumed as 1.22 kg m^{-3} and the drag coefficient $\boldsymbol{C_D}$ is computed using the formulation of Yelland and Taylor (1996); $\boldsymbol{u}$ and $\boldsymbol{v}$ are the zonal (eastward) and meridional (northward) wind speed components respectively; $\boldsymbol{\alpha}$ and $\boldsymbol{\beta}$ are the angles between the wind speed components and the coastal orientation and in this case both of them are assumed to be 45° because of the orientation of the coast in our study area.

The monsoon intensity has been defined by different climate indices that capture different aspects of the monsoon variability. Here, we use monsoon indices taken from the literature that are based on low-tropospheric winds over South Asia or Indian precipitation. With this analysis, however, we do not imply that precipitation, for instance, may be a direct driver of Arabian Sea upwelling. In order to estimate the statistical relationship between upwelling and the Monsoon, we employ the wind-based Indian Monsoon index (IMI) defined by Wang and Fan (1999) and the All India Monsoon rainfall index (IMR) from the Indian Institute of Tropical Meteorology (Parthasarathy et al. 1994) as well as the Webster and Yang monsoon index (WYM) defined by Webster and Yang (1992) also defined in terms of wind speed. We calculate the IMI and WYM based on wind speed from NCEP/NCAR reanalysis while the IMR is obtained from station rainfall records in India. In addition, several other meteorological and oceanic variables are also investigated. Surface air temperature (ST) data and sea level pressure (SLP) data from the NCEP/NCAR reanalysis are investigated to provide further understanding. Because of a continuity issue in the STORM simulation output (missing data in year 1949), we limit the study period from 1950 to 2010. The only datasets not covering this whole period are AVHRR SST data (1985-2009), CCMP winds (1988-2010), and the IMR record (1950-2000).

Since the model has already been globally analysed and assessed (von Storch et al. 2012), we hereby present the information of the modelled mixed layer depth (MLD) and the comparison between the modelled SST and the observational SST from AVHRR. Figure 2 shows that the simulated MLD is shallower along the coast than in the open sea and that the MLD in the upwelling region is slightly deeper during the upwelling season than during the pre- or post- upwelling season, although the mixed layer is clearly deepest during the winter season. In general, the modelled MLD is comparable with the MLD climatology derived by de Boyer Montégut et al. (2004) and that the MLD attains a relative maximum during the upwelling season is a reasonable result as described by Murtugudde et al.

(2007). The shallowing of MLD caused by upwelling is counteracted by strong surface turbulent kinetic energy and entrainment cooling, which tend to deepen the MLD. The SSTs from STORM and AVHRR are compared in Fig. 3. In general, the SST from STORM is cooler than that from AVHRR in the upwelling region but they display good correlation (r=0.51) and even better correlation in the open sea, which indicates that the model is capable to simulate the observed variabilities. Note that the coastal SST bias between model and the observation may exceed 5°C. This bias is admittedly large, but it is within the SST biases found across the CMIP5 climate models in the coastal upwelling regions in the EBUSs (Richter 2015) and also across the CMIP3 models for the Arabian Sea in the winter season (Marathayil et al. 2013). A recent study based on CMIP5 models also shows cold bias in the Arabian Sea SST during summer (Sayantani et al. 2016). Therefore, the bias detected in the STORM simulation, though large, does not seem to be an outlier among other models. It also indicates that the higher model resolution of STORM compared to the CMIP5 models (10 km versus typically 100 km) is not decisive to reduce the SST bias. The reason for this bias remains, therefore, unexplained and is likely not an artifact of STORM alone, but runs across the whole climate model ensemble. The correct simulation of the mean SST in tropical coastal regions remains a challenge for most global models.

3. Coastal Upwelling in the Western Arabian Sea

Upwelling along the west coast of the Arabian Sea usually starts in May and ends in September (Brock et al. 1991). This is well reproduced in the modelled annual cycle of the upwelling velocity (Fig. 4a), which is converted from the original model output of upward water mass transport. Here, positive values indicate upwelling whereas negative values indicate downwelling. The annual cycle of the upwelling velocity shows that the significant positive values start from May, peak in July and end in September. As one of the traditional upwelling indices, the south-west (SW) wind-stress (Fig. 4b) is in good consistency with the upwelling velocity with a peak in July as well. Another traditional upwelling index is the observed coastal SST. Our modelled SST (Fig. 4c) also reveals good correlation with the upwelling velocity with a lag of approximately one month. This lag can be explained by the time needed to transport deeper and cooler water to the surface and it matches a similar lag between wind-stress and SST found in the observations by Rixen et al. (2000). It is obvious that the ranges of these three annual cycles tend to get larger when the upwelling becomes stronger. Therefore, unless indicated otherwise, when referring to summer period in the following analyses, we average the values from June to August (JJA) for all the variables except SST which is selected from July to September (JAS) due to the previously mentioned lag time.

The selected coastal upwelling band (Fig. 1) is very narrow but the high resolution of the STORM simulation means it can reproduce the spatial patterns of the upwelling in the study domain. The simulated mean upwelling velocity averaged over this domain in JJA from 1950 to 2010 is about 1.8 m day^{-1}. Upwelling is less intense in the area north to Ras Madrakah and much stronger at regions near the capes such as Sawqirah and Nishtun where the velocity can exceed 6 m day^{-1} at some model grid-cells. These velocities appear compatible with the estimation of the high range of the vertical velocity estimated by Shi et al. (2000) from altimetry data of about 2.5 m day^{-1}, considering the coarser resolution of the satellite data relative to our ocean model. In addition, we conduct an estimation of the upwelling velocity induced by the Ekman transport to verify our modelled upwelling velocity. We use the simple equations described by Rykaczewski and Checkley (2008) to calculate the coastal upwelling velocity caused by Ekman transport. The estimated mean upwelling velocity induced by Ekman transport is about 4 m day^{-1}, which is within the same order of magnitude of the modelled upwelling velocity. This shows that the model produces reasonable result because the upwelling along the western coast of the Arabian Sea is caused by the SW wind-stress through Ekman transport.

4. Upwelling Variability

For an understanding about the spatial variability of upwelling in this region, we calculate the standard deviation (STD) and perform an Empirical Orthogonal Function (EOF) analysis (von Storch and Zwiers 2001) of the upwelling velocity. The STD map (Fig. 5a) shows that higher mean intensity of upwelling comes with higher variance, that is, in the regions where the upwelling velocity is higher (Fig. 1), the STD of the upwelling velocity is also higher. The mean STD over the entire study area is about 0.7 m day^{-1}, which is nearly half of the mean upwelling velocity.

The EOF analysis is a method that identifies the main spatial patterns of coherent variation. This method identifies spatial patterns that describe most of the data variance and that display uncorrelated temporal evolutions. In our case, the leading mode arising from the EOF analysis (Fig. 5b) reveals apparent coastal-offshore pattern and accounts for only 10% of the total variance and cannot be separated from the second mode according to the North's rule (North et al. 1982). In addition, the first principal component (PC1) time series is highly consistent with the spatially averaged upwelling velocity ($r = 0.82$, shown in Fig. 6b), which indicates that the only 10% of the variance evolves coherently and contributes to the spatially averaged upwelling, mostly along the coastal regions, while the remaining 90% of variance over the whole region is affected by local processes. Therefore, the high STD with respect to the mean value of upwelling velocity and the low explained variance from the leading mode of the EOF analysis together indicate that the upwelling in this region is spatially very heterogeneous and must be affected by various and complex processes. A dominating influence by one single mechanism, for instance, the Monsoon, would give rise to a leading pattern describing a much higher portion of variance. This spatially heterogeneous variability of simulated upwelling confirms the findings derived from surface chlorophyll concentrations as an indirect indicator of upwelling (Piontkovski and Al-Jufaili 2013) and modelling results with a high-resolution regional model (L'Hégaret et al. 2015). The high mesoscale variability mainly arises in that model simulation by the generation of Rossby waves along the Indian coast, which may affect the upper 1000 meters in that model. Although the detailed analysis of the mesoscale variability in the STORM simulation is outside the scope of the present study, it is reasonable to assume that the high spatial variability in STORM in this region may be generated by similar mechanisms.

Beside the spatial variability, we also look at the temporal variability of upwelling. The primary attempt is to investigate any trend in the upwelling time series referring to the Bakun hypothesis (Bakun 1990) that coastal upwelling should intensify as a consequence of anthropogenic greenhouse gas forcing at global scale. This hypothesis has been contested and recent studies have shown both supportive (Sydeman et al. 2014) and unsupportive (Tim et al. 2015) results regarding the long term trends. In our study, however, only a nonsignificant positive trend (p-value = 0.1954) is revealed over the last 61 years (Fig. 6a). This trend has a slope of 0.0035 m day^{-1} per year, which over the 60 years of simulation would imply an increase of about only 12% of the mean coastal upwelling velocity in the domain. Hence, although the trend may physically exist, it cannot be distinguished from a spurious trend caused by stochastic variability. In addition, there are also no significant trends that can be identified in our SST and wind data, comparing to the results of previous studies based on SST (Liao et al. 2015) and wind (Varela et al. 2015). Thus we do not further discuss about trends in the following text. However, although the trend is not statistically significant due to its magnitude relative to the interannual variability and to the short length of the simulation, we detrend all variables in the subsequent correlation analysis to avoid that these correlations maybe contaminated by long-term trends that might not necessarily be physically related.

We compare the time series of the upwelling velocity with SST and the SW wind-stress to validate our modelled upwelling data since they are generally applied as coastal upwelling indices (Fig. 6b, 6c, and 6d). The time series of upwelling and SST are generated using data within the upwelling domain shown in Fig. 1 while the SW wind-stress time series contains data from a broader area due to the low resolution of the wind data. In Fig. 6b, the upwelling velocity and the PC1 time series from the EOF analysis are compared with SST from the STORM simulation and the SW wind-stress from the NCEP/NCAR reanalysis. The comparison reveals that the upwelling is strongly negatively correlated to the SST ($r = -0.83$) as well as positively to the SW wind-stress ($r = 0.73$). In addition, we also compared our upwelling time series with the indices of the Indian Ocean Basin mode (IOB), Indian Ocean Dipole mode (IOD) and El Niño/Southern Oscillation (ENSO) but no significant correlations could be found. Thus, the effect of the IOB, the IOD and ENSO are very limited on the simulated Arabian Sea upwelling.

Note that the high correlation between the SST and the upwelling does not necessarily mean that the upwelling directly dominates the SST variability through vertical advection. SST variability could additionally be modulated by the surface energy fluxes, which in turn are also modulated by the wind through latent and sensible heat. We calculate the latent and sensible heat fluxes from the NCEP/NCAR reanalysis in our study area for the upwelling season and find that the upwelling and the SW wind-stress are correlated with the surface heat fluxes at a similar level. The regression coefficients between the SW wind-stress and the heat fluxes show that the upwelling favourable (southerly) wind is linked to increased latent heat loss from the ocean surface and also to stronger sensible heat into the ocean. The cooling effect, as estimated from the regression coefficient, is about three times larger than the warming effect, so that the surface heat fluxes also contribute to cool the ocean surface. However, it is difficult to separate and determine whether the upwelling or the SW wind-stress plays a more important role in affecting the SST variability, since upwelling itself also modulates the surface energy fluxes as it modifies the SSTs. A quantitative estimation of the sole effect of vertical advection on SSTs requires the computation of heat transport by the seasonal mean circulation and by the mesoscale variations, but it lies outside the scope of this study.

Since the SST and the upwelling velocity are both outputs from the STORM simulation and the NCEP wind data is the forcing used in this simulation, these high correlations are to some extent expected and less persuasive without the support from extra sources. Therefore, we employ wind data from CCMP and SST data from AVHRR (Fig. 6c and 6d) as they are independent of the STORM simulation, although their temporal coverages are shorter than

STORM. The correlations between simulated upwelling and these two observed variables are lower (wind r = 0.49 and SST r = -0.45) but they remain significant at the 95% level or higher as in the previous analysis.

These analyses suggest that the results of the STORM simulation are rather consistent with the observations, and more importantly, the upwelling velocity derived from the STORM simulation is significantly consistent with the traditional upwelling indices, and so it is reasonable to use it for further studies such as investigating the responsible processes affecting the upwelling.

5. Link to the Indian Monsoon

As it has been suggested that the ISM is strongly linked to upwelling in the western Arabian Sea, we examine the relationship between the simulated upwelling velocity and the Indian Monsoon index (IMI), all India Monsoon rainfall index (IMR) and Webster and Yang monsoon index (WYM) in Fig. 7. Note that the IMR is computed by integrating the total rainfall records of numerous stations from June to September (JJAS) and the data source is not available for single months. Thus, we calculate the IMI and the WYM and also the upwelling velocity for the extended JJAS season. All of the three comparisons show low and negative correlations in the northern part of the domain. Higher correlations are found along the coast and to the south especially the regions with more intense upwelling and larger variance, but only a few areas show correlations that pass the significance level of 95%.

One interesting finding is that the correlation patterns obtained with IMI (Fig. 7a) and with IMR (Fig. 7b) are quite similar. The correlations start to become positive at Ras Madrakah and the highest and the most significant correlations are located between Sawqirah and Nishtun. In addition, the areas with stronger correlation and higher significance strongly overlap. Considering the fact that IMI is calculated from the difference of two wind-speed fields whereas IMR is obtained from the rainfall records, this similarity indicates that the upwelling has very similar link to the variation of the wind-speed and the rainfall. These links likely arise through the large-scale patterns that drive climate anomalies in this region, but do not imply that rainfall is a dynamical driver of upwelling.

The WYM correlation pattern (Fig. 7c) shows a different structure, with positive values that begin to appear from the north of Ras Madrakah and the strongest and most significant correlation lies between Ras Madrakah and Nishtun. Although WYM is also calculated from the difference of two wind-speed fields, the strategies for selecting the fields are not the same and this is causing the difference between the patterns of IMI and WYM. Additionally, the two wind-based indices, IMI and WYM, capture reduced correlations near Salalah but IMR does not.

The spatially heterogeneous correlations indicate that the upwelling velocities in different regions along the western Arabian Sea coast are sensitive to different forcing mechanisms. Furthermore, it is surprising that the overall correlations of upwelling with all monsoon indices are rather low and insignificant. With regards to the STORM simulation, therefore, this analysis indicates that the impact of the ISM on western Arabian Sea coastal upwelling is weak and limited to areas with upwelling of higher intensity (Fig. 1) and variability (Fig. 5a).

6. Relationship with Sea Level Pressure and Surface Air Temperature

In order to determine the other possible large-scale atmospheric patterns that could influence the variability of upwelling, we study the SLP (Fig. 8) and ST (Fig. 9) field in the broader Asian (Indian Ocean) region. SLP and ST are both reported to be highly associated with the ISM although their relationships with upwelling have not been directly studied yet. Figure 8a shows the mean summer SLP, with the low pressure zone over the Arabian Sea and Indian subcontinent is surrounded by the high pressure zones. The gradient between the high pressure and the low pressure zones contributes to the formation of the ISM. The leading mode of the EOF analysis of SLP (Fig. 8b), which describes a large part of the SLP variability (61%) indicates that the variation of SLP over the ocean and the continent tend to be in phase, which means the variability of the ocean-continent SLP gradient is not large. The first principal component from the EOF analysis of upwelling, PC1 will be used as an index of upwelling in the following analyses. In Fig. 8c we correlate the PC1 with the SLP field to gain an insight between the relationship of the upwelling variability and the SLP field. The pattern of correlations displays the positive correlations over the Arabian Sea and the negative correlations over the Himalayas. We also take one of the monsoon indices, the IMI, to correlate with the SLP field (Fig. 8d). With negative correlations over the Arabian Sea and positive correlations over Himalayas, the IMI shows different connections with the SLP field compared to the correlation pattern derived from the upwelling PC1. Thus, the upwelling PC1 is well correlated to the SW wind generated by the gradient of the SLP field, which is also found in Section 4. However, in contrast to the upwelling PC1, the IMI is not linked to this gradient, which might explain the poor correlation between upwelling and the monsoon indices found in Section 5.

Since the seasonality of the Indian Monsoon is thought to be mainly driven by the temperature contrasts between land and Indian Ocean, the same analysis is performed on the ST field. The JJA mean ST map (Fig. 9a) shows that the lower temperature dominates the Tibetan Plateau, where also the high SLP is located (Fig. 8a). The leading EOF mode of ST (Fig. 9b) shows that the temperature in northern India and temperature in central India tend to be anticorrelated. The correlations between ST and upwelling PC1 (Fig. 9c) and the correlation between ST and IMI (Fig. 9d) also reveal correlations of opposite signs in these two regions. Thus, according to the EOF analysis, in the years in which the central Indian is colder than northern India, the upwelling and the ISM tend to be more intense. The upwelling PC1 has a similar link to the ST as the IMI although the IMI has more significant correlations. Thus, the relationships between upwelling and temperature and the ISM and temperature are much more similar than in the case of SLP.

Therefore, we have found that upwelling and Monsoon are connected to different SLP patterns, but both are linked to similar temperature patterns over this part of Asia. This can explain why upwelling may have been considered in the past to be closely related to the Monsoon. The physical explanation that we suggest here is that the SLP pattern related to upwelling is physically linked to stronger westerly winds over the Arabian Sea and a stronger advection of maritime air masses from the Arabian Sea into the Indian subcontinent, causing lower temperatures there. In contrast, as it is well known, the Monsoon is connected to higher rainfall over India, with increased cloudiness, less solar radiation, and therefore also lowers temperatures over the Indian subcontinent. Thus, the physical reasons for the lower temperatures in India in years with stronger Monsoon and in years with stronger upwelling are physically different. The same physical reasoning can be applied in years with weaker upwelling or weaker Monsoon, respectively.

7. Discussion and Conclusions

In this study we use the upwelling simulated by a high-resolution global ocean simulation over the past decades to identify the atmospheric drivers of upwelling along the west coast of the Arabian Sea. With significantly improved spatial resolution, our modelled upwelling velocity presents consistent annual cycle with the traditional upwelling indices.

One limitation of our study that has to be borne in mind is the degree of realism of the ocean model used. Another possible limitation is the realism of the atmospheric forcing (NCEP/NCAR meteorological reanalysis) used to drive the ocean model. It is difficult to validate the simulated upwelling against direct observations of vertical velocities, and thus we have to rely on indirect analysis. Here, we showed that the link between simulated upwelling and SSTs, and the correlation between simulated upwelling and independent wind-stress data suggest a reasonable degree of realism of the ocean simulation. Also, the annual cycle of the depth of the mixed layer and the spatial heterogeneity of upwelling is compatible with the limited available information from observations.

One conclusion of our study is that in general, no significant long-term trend is detected in the upwelling time series, although this may be due to the short length of the simulation and the small magnitude of the possible long-term trend relative to the interannual variations.

The upwelling intensity and variability are found to be higher along the southern coast than along the northern coast of Oman. This result suggests that upwelling along the southern coast is more intense. In addition, the southern coast is also the region where upwelling is most significantly connected to the ISM but the correlation between them is not as high as expected from previous studies. Therefore, this simulation does not reveal a strong impact of the Indian Monsoon on the western Arabian Sea coastal upwelling.

This low correlation points to other processes that might contribute to the upwelling variability. Both SLP and ST are considered and are compared with the upwelling PC1. The comparisons indicate that the upwelling is strongly affected by the SLP gradient between the Himalayas and the Arabian Sea and is also linked to the ST gradient between northern and central India. These two gradients, however, are also connected to the Monsoon (Feng and Hu 2005; Krishnamurthy and Ajayamohan 2010) so caution should be taken when distinguishing the sources that influence the upwelling. On one hand, the upwelling is weakly correlated to the ISM but significantly correlated to the SLP and the ST gradients; on the other hand, both of the SLP and the ST gradients are associated with the ISM. The contrast and the consistency of the relationship between upwelling PC1 and IMI in their correlations with SLP and ST indicate that the link between Monsoon and ST and between upwelling and ST display similar spatial structures, whereas in the case of SLP the correlation patterns are quite different. The physical explanation is that the SLP pattern that drives upwelling in the Arabian Sea is statistically linked to a similar temperature pattern over India that also tend to appear with the Monsoon. The physical connections are, however, different. Whereas the SLP pattern related to upwelling advects cold temperatures from the Arabian Sea into India, the Monsoon is linked to lower temperatures there likely due to higher rainfall and cloudiness.

The lack of long-term observational data restricts the validation of the results and the data from satellite ocean-colour observations are heavily blocked during the upwelling season in the Arabian Sea. Methods such as the one described by Banzon et al. (2004) will help to recover the gaps in the satellite data and thus the recovered data might be possible to further inspect the results in this study.

References

Anderson DM, Brock JC, Prell WL (1992) Physical upwelling processes, upper ocean environment and the sediment record of the southwest monsoon. Geol Soc Sp 64:121-129 doi:10.1144/gsl.sp.1992.064.01.08

Anderson DM, Overpeck JT, Gupta AK (2002) Increase in the Asian Southwest Monsoon During the Past Four Centuries. Science 297:596-599 doi:10.1126/science.1072881

Atlas R, Hoffman RN, Ardizzone J, Leidner SM, Jusem JC, Smith DK, Gombos D (2011) A Cross-calibrated, Multiplatform Ocean Surface Wind Velocity Product for Meteorological and Oceanographic Applications. B Am Meteorol Soc 92:157-174 doi:10.1175/2010BAMS2946.1

Bakun A (1973) Coastal upwelling indices, west coast of North America, 1946-71. NOAA Technical Report NMFS SSRF-671

Bakun A (1990) Global Climate Change and Intensification of Coastal Ocean Upwelling. Science 247:198-201 doi:10.1126/science.247.4939.198

Banzon VF, Evans RE, Gordon HR, Chomko RM (2004) SeaWiFS observations of the Arabian Sea southwest monsoon bloom for the year 2000. Deep Sea Res Part II 51:189-208 doi:10.1016/j.dsr2.2003.10.004

Brock JC, McClain CR (1992) Interannual variability in phytoplankton blooms observed in the northwestern Arabian Sea during the southwest monsoon. J Geophys Res Oceans 97:733-750 doi:10.1029/91JC02225

Brock JC, McClain CR, Luther ME, Hay WW (1991) The phytoplankton bloom in the northwestern Arabian Sea during the southwest monsoon of 1979. J Geophys Res Oceans 96:20623-20642 doi:10.1029/91JC01711

Casey KS, Brandon TB, Cornillon P, Evans R (2010) The Past, Present, and Future of the AVHRR Pathfinder SST Program. In: Barale V, Gower JFR, Alberotanza L (eds) Oceanography from Space: Revisited. Springer Netherlands, Dordrecht, pp 273-287. doi:10.1007/978-90-481-8681-5_16

Curry WB, Ostermann DR, Guptha MVS, Ittekkot V (1992) Foraminiferal production and monsoonal upwelling in the Arabian Sea: evidence from sediment traps. Geol Soc Sp 64:93-106 doi:10.1144/gsl.sp.1992.064.01.06

de Boyer Montégut C, Madec G, Fischer AS, Lazar A, Iudicone D (2004) Mixed layer depth over the global ocean: An examination of profile data and a profile-based climatology J Geophys Res Oceans 109:n/a-n/a doi:10.1029/2004JC002378

deCastro M, Sousa MC, Santos F, Dias JM, Gómez-Gesteira M (2016) How will Somali coastal upwelling evolve under future warming scenarios? Scientific Reports 6:30137 doi:10.1038/srep30137

Emeis K-C, Anderson DM, Doose H, Kroon D, Schulz-Bull D (1995) Sea-Surface Temperatures and the History of Monsoon Upwelling in the Northwest Arabian Sea during the Last 500,000 Years. Quaternary Res 43:355-361 doi:10.1006/qres.1995.1041

Feng S, Hu Q (2005) Regulation of Tibetan Plateau heating on variation of Indian summer monsoon in the last two millennia. Geophys Res Lett 32 doi:10.1029/2004GL021246

Findlater J (1969) A major low-level air current near the Indian Ocean during the northern summer. Q J Roy Meteor Soc 95:362-380 doi:10.1002/qj.49709540409

Godad SP, Naidu PD, Malmgren BA (2011) Sea surface temperature changes during May and August in the western Arabian Sea over the last 22 kyr: Implications as to shifting of the upwelling season. Mar Micropaleontol 78:25-29 doi:10.1016/j.marmicro.2010.09.006

Izumo T, Montégut CB, Luo J-J, Behera SK, Masson S, Yamagata T (2008) The Role of the Western Arabian Sea Upwelling in Indian Monsoon Rainfall Variability. J Climate 21:5603-5623 doi:10.1175/2008JCLI2158.1

Jacox MG, Moore AM, Edwards CA, Fiechter J (2014) Spatially resolved upwelling in the California Current System and its connections to climate variability. Geophys Res Lett 41:3189-3196 doi:10.1002/2014GL059589

Kalnay E et al. (1996) The NCEP/NCAR 40-Year Reanalysis Project. B Am Meteorol Soc 77:437-471 doi:10.1175/1520-0477(1996)077<0437:TNYRP>2.0.CO;2

Krishnamurthy V, Ajayamohan RS (2010) Composite Structure of Monsoon Low Pressure Systems and Its Relation to Indian Rainfall. J Climate 23:4285-4305 doi:10.1175/2010JCLI2953.1

Kroon D, Steens T, Troelstra SR (1991) Onset Of Monsoonal Related Upwelling In The Western Arabian Sea As Revealed By Planktonic Foraminifers. Proc Ocean Drill Program Sci Results 117:257-263 doi:10.2973/odp.proc.sr.117.126.1991

L'Hégaret P, Duarte R, Carton X, Vic C, Ciani D, Baraille R, Corréard S (2015) Mesoscale variability in the Arabian Sea from HYCOM model results and observations: impact on the Persian Gulf Water path. Ocean Sci 11:667-693 doi:10.5194/os-11-667-2015

Liao E, Lu W, Yan X-H, Jiang Y, Kidwell A (2015) The coastal ocean response to the global warming acceleration and hiatus Scientific Reports 5:16630 doi:10.1038/srep16630

Ma J, Liu H, Lin P, Zhan H (2014) Seasonality of biological feedbacks on sea surface temperature variations in the Arabian Sea: The role of mixing and upwelling. J Geophys Res Oceans 119:7592-7604 doi:10.1002/2014JC010186

Manghnani V, Morrison JM, Hopkins TS, Böhm E (1998) Advection of upwelled waters in the form of plumes off Oman during the Southwest Monsoon. Deep Sea Res Part II 45:2027-2052 doi:10.1016/S0967-0645(98)00062-9

Marathayil D, Turner AG, Shaffrey LC, Levine RC (2013) Systematic winter sea-surface temperature biases in the northern Arabian Sea in HiGEM and the CMIP3 models Environmental Research Letters 8:014028

Murtugudde R, Seager R, Thoppil P (2007) Arabian Sea response to monsoon variations. Paleoceanography 22 doi:10.1029/2007PA001467

Naik SS, Godad SP, Naidu PD, Ramaswamy V (2013) A comparison of Globigerinoides ruber calcification between upwelling and non-upwelling regions in the Arabian Sea. J Earth Syst Sci 122:1153-1159 doi:10.1007/s12040-013-0330-y

Narayan N, Paul A, Mulitza S, Schulz M (2010) Trends in coastal upwelling intensity during the late 20th century. Ocean Sci 6:815-823 doi:10.5194/os-6-815-2010

North GR, Bell TL, Cahalan RF, Moeng FJ (1982) Sampling Errors in the Estimation of Empirical Orthogonal Functions Monthly Weather Review 110:699-706 doi:10.1175/1520-0493(1982)110<0699:SEITEO>2.0.CO;2

Parthasarathy B, Munot AA, Kothawale DR (1994) All-India monthly and seasonal rainfall series: 1871–1993. Theor Appl Climatol 49:217-224 doi:10.1007/bf00867461

Piontkovski SA, Al-Jufaili S (2013) Coastal upwellings and Mesoscale Eddies of the Western Arabian Sea: Some Biological Implications. Int J Ocean Oceanogr 7:93-115

Prell W, Curry W (1981) Faunal and isotopic indices of monsoonal upwelling-western Arabian Sea. Oceanol Acta 4:91-98

Prell WL, van Campo E (1986) Coherent response of Arabian Sea upwelling and pollen transport to late Quaternary monsoonal winds. Nature 323:526-528 doi:10.1038/323526a0

Rao AD, Joshi M, Ravichandran M (2008) Oceanic upwelling and downwelling processes in waters off the west coast of India. Ocean Dynam 58:213-226 doi:10.1007/s10236-008-0147-4

Richter I (2015) Climate model biases in the eastern tropical oceans: causes, impacts and ways forward Wiley Interdisciplinary Reviews: Climate Change 6:345-358 doi:10.1002/wcc.338

Rixen T, Haake B, Ittekkot V (2000) Sedimentation in the western Arabian Sea the role of coastal and open-ocean upwelling. Deep Sea Res Part II 47:2155-2178 doi:10.1016/S0967-0645(00)00020-5

Rykaczewski RR, Checkley DM (2008) Influence of ocean winds on the pelagic ecosystem in upwelling regions Proceedings of the National Academy of Sciences 105:1965-1970 doi:10.1073/pnas.0711777105

Sayantani O, Gnanaseelan C, Chowdary JS, Parekh A, Rahul S (2016) Arabian Sea SST evolution during spring to summer transition period and the associated processes in coupled climate models Int J Climatol 36:2541-2554 doi:10.1002/joc.4511

Shi W, Morrison JM, Böhm E, Manghnani V (2000) The Oman upwelling zone during 1993, 1994 and 1995. Deep Sea Res Part II 47:1227-1247 doi:10.1016/S0967-0645(99)00142-3

Sydeman WJ, García-Reyes M, Schoeman DS, Rykaczewski RR, Thompson SA, Black BA, Bograd SJ (2014) Climate change and wind intensification in coastal upwelling ecosystems. Science 345:77-80 doi:10.1126/science.1251635

Tim N, Zorita E, Hünicke B (2015) Decadal variability and trends of the Benguela upwelling system as simulated in a high-resolution ocean simulation. Ocean Sci 11:483-502 doi:10.5194/os-11-483-2015

Tozuka T, Nagura M, Yamagata T (2014) Influence of the Reflected Rossby Waves on the Western Arabian Sea Upwelling Region. J Phys Oceanogr 44:1424-1438 doi:10.1175/JPO-D-13-0127.1

Varela R, Álvarez I, Santos F, deCastro M, Gómez-Gesteira M (2015) Has upwelling strengthened along worldwide coasts over 1982-2010? Scientific Reports 5:10016 doi:10.1038/srep10016 von Storch H, Zwiers FW (2001) Statistical Analysis in Climate Research. Cambridge University Press, Cambridge, UK

von Storch J-S et al. (2012) An Estimate of the Lorenz Energy Cycle for the World Ocean Based on the STORM/NCEP Simulation. J Phys Oceanogr 42:2185-2205 doi:10.1175/JPO-D-12-079.1

Wang B, Fan Z (1999) Choice of South Asian Summer Monsoon Indices. B Am Meteorol Soc 80:629-638 doi:10.1175/1520-0477(1999)080<0629:COSASM>2.0.CO;2

Wang D, Gouhier TC, Menge BA, Ganguly AR (2015) Intensification and spatial homogenization of coastal upwelling under climate change. Nature 518:390-394 doi:10.1038/nature14235

Webster PJ, Yang S (1992) Monsoon and Enso: Selectively Interactive Systems. Q J Roy Meteor Soc 118:877-926 doi:10.1002/qj.49711850705

Yelland M, Taylor PK (1996) Wind Stress Measurements from the Open Ocean. J Phys Oceanogr 26:541-558 doi:10.1175/1520-0485(1996)026<0541:WSMFTO>2.0.CO;2

Figure captions

Fig.1 Summer mean upwelling velocity (m day^{-1}) from 1950 to 2010. The coastal region surrounded by the red line shows the study area

Fig.2 (a) Summer mean mixed-layer depth (MLD) (m) from 1950 to 2010. (b) Annual cycle of MLD (m) in the study area. (c) Time series of summer mean MLD (m) in the study area (1950-2010)

Fig.3 (a) Summer mean SST (°C) from STORM. (b) Summer mean SST (°C) from AVHRR. (c) Summer mean SST difference (°C) between STORM and AVHRR. (d) Summer mean SST correlation (r) between STORM and AVHRR. Areas within the green contours are statistically significant at the 95% level or higher. The time period is chosen from 1985 to 2009 to be consistent with AVHRR. The plot in (d) shows the 25-year time series of the summer mean SSTs (°C) from STORM and AVHRR in the study area

Fig.4 Annual cycle of (a) upwelling velocity (m day^{-1}), (b) SW wind-stress (N m^{-2}) and (c) SST (°C) averaged for the study area. Colour shaded areas are the ranges of the annual cycles and grey shaded months are the study periods selected for each variable

Fig.5 (a) Standard deviation of the summer mean upwelling velocity (STD) (m day^{-1}) from 1950 to 2010. (b) Leading mode of the EOF analysis of the summer mean upwelling velocity which accounts for only 10% of the variance

Fig.6 (a) Time series of summer mean upwelling velocity (m day^{-1}) and its long term trend from 1950 to 2010. (b) Time series comparison of summer mean upwelling velocity, upwelling PC1, SW wind-stress from NCEP and SST from STORM (1950-2010). (c) Time series of summer mean upwelling velocity and SW wind-stress from CCMP (1988-2010). (d) Time series of summer mean upwelling velocity and SST from AVHRR (1985-2009). All the time series are calculated by averaging the values within the study area and the ones in (b), (c) and (d) are detrended and normalized for their spanning time periods

Fig.7 Correlations (r) between summer mean upwelling velocity and several Monsoon indices: (a) IMI, (b) IMR as well as (c) WYM indices. Green contours encompass the areas where correlations are significant at the 95% level or higher. The plots to the right of each map show the zonal mean correlation coefficient between each monsoon index and the summer mean upwelling velocity averaged within the study area. The upper dashed lines indicate the general starting points of the positive correlations and between the middle and the lower dashed lines are the areas where the correlations are the highest

Fig.8 (a) Summer mean SLP (hPa) from 1950 to 2010. (b) Leading mode of the EOF analysis on the summer mean SLP which accounts for 61% of the variance. (c) Correlation (r) between upwelling PC1 and summer mean SLP. (d) Correlation between IMI and summer mean SLP. The green contours delimit the areas where the correlations are significant at the 95% level or higher

Fig.9 (a) Summer mean ST (°C) from 1950 to 2010. (b) Leading mode of the EOF analysis on the summer mean ST which accounts for 31% of the variance. (c) Correlation (r) between upwelling PC1 and summer mean surface temperature (ST). (d) Correlation between IMI and summer mean ST. The green contours delimit the areas where the correlations are significant at the 95% level or higher

Figure 1

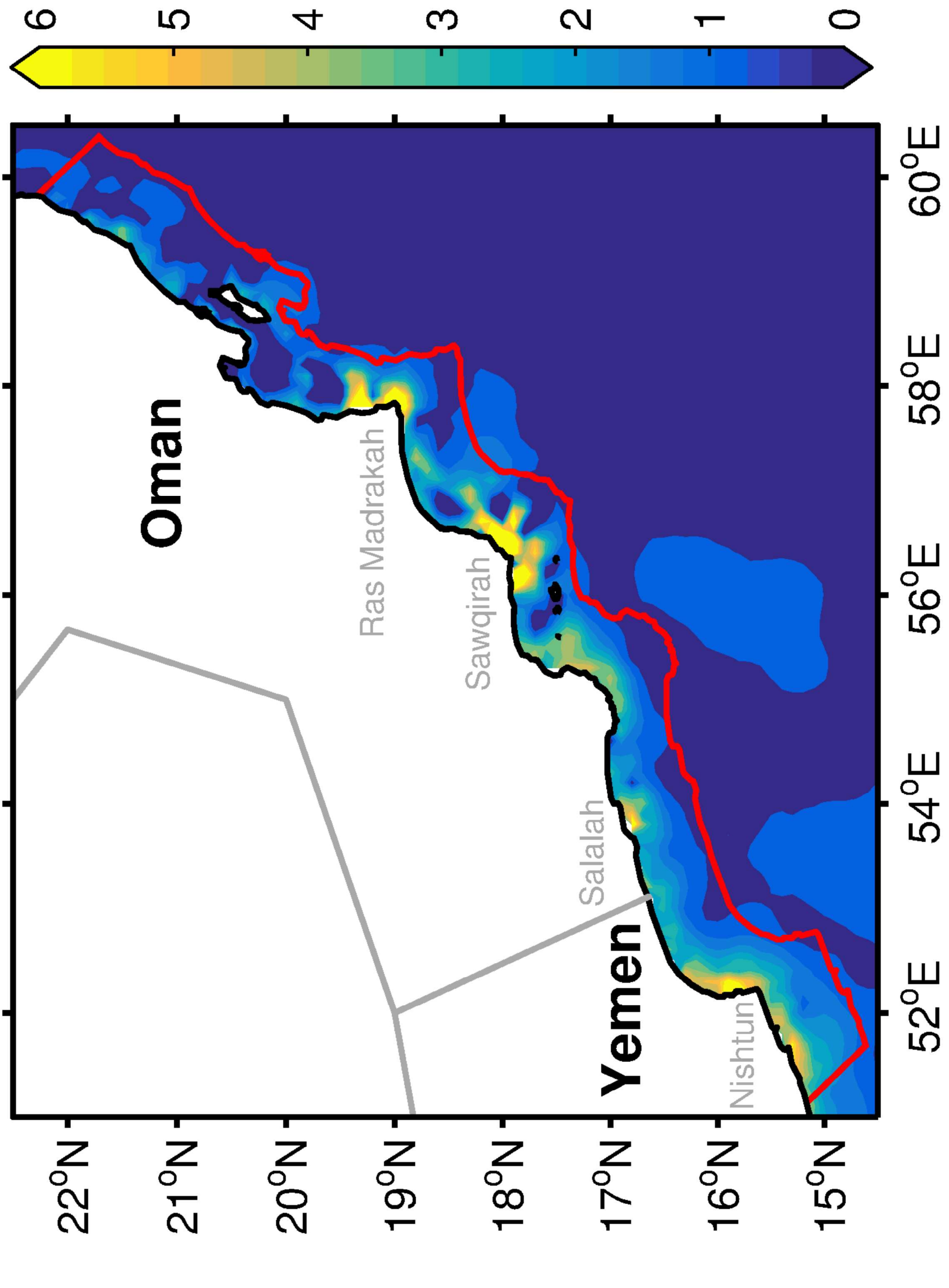

Oman
Yemen
Ras Madrakah
Sawqirah
Salalah
Nishtun
22°N
21°N
20°N
19°N
18°N
17°N
16°N
15°N
52°E
54°E
56°E
58°E
60°E
0
1
2
3
4
5
6

Figure 2

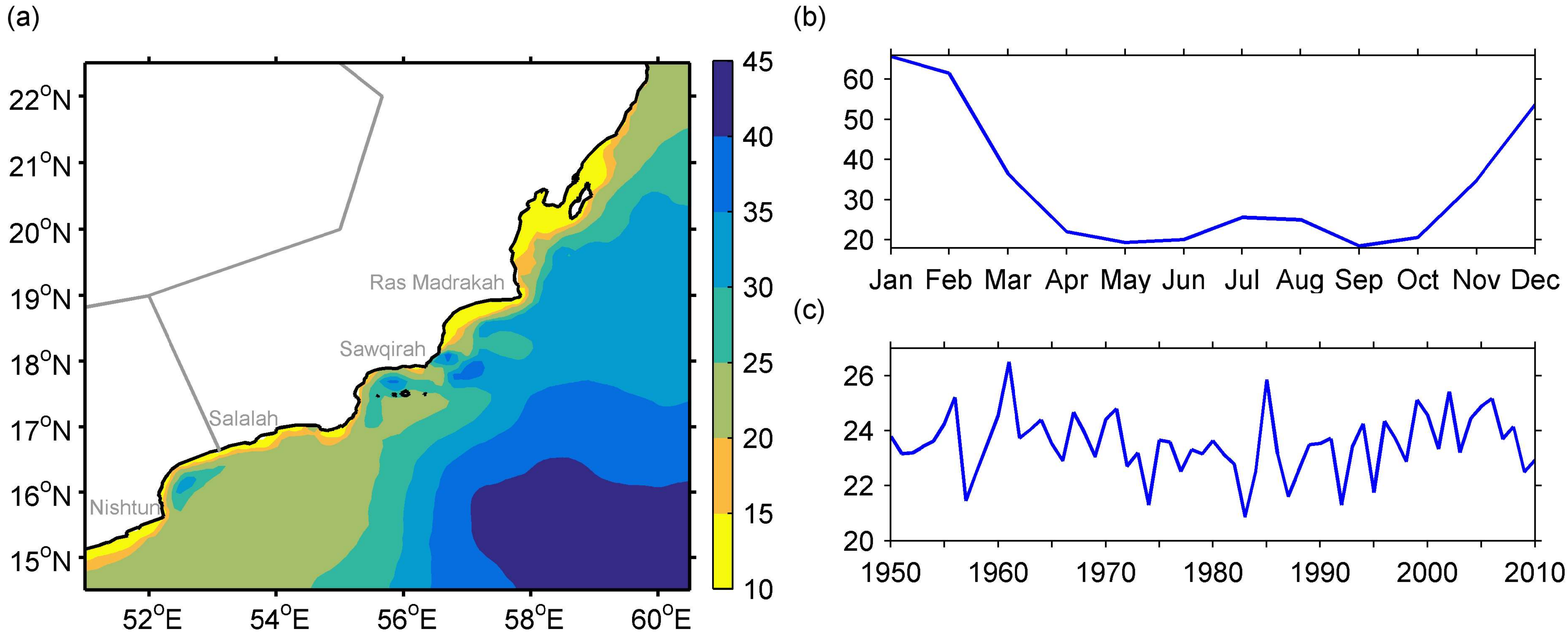
(a)
22°N
21°N
20°N
19°N
18°N
17°N
16°N
15°N
52°E
54°E
56°E
58°E
60°E
Ras Madrakah
Sawqirah
Salalah
Nishtun
45
40
35
30
25
20
15
10
(b)
60
50
40
30
20
Jan Feb Mar Apr May Jun Jul Aug Sep Oct Nov Dec
(c)
26
24
22
20
1950
1960
1970
1980
1990
2000
2010

Figure 3

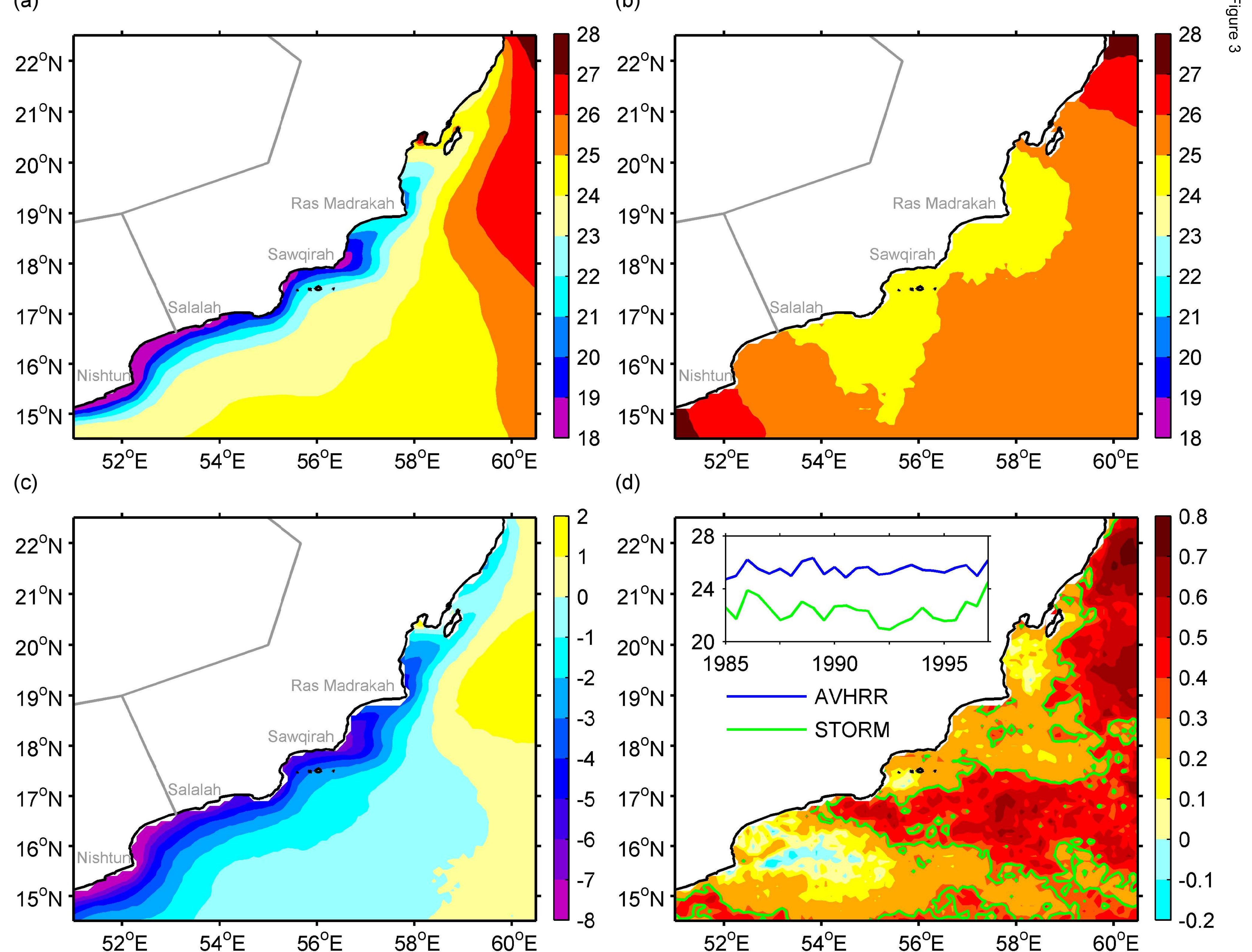
(a)
(b)
(c)
(d)
Ras Madrakah
Sawqirah
Salalah
Nishtun
22°N
21°N
20°N
19°N
18°N
17°N
16°N
15°N
52°E
54°E
56°E
58°E
60°E
28
27
26
25
24
23
22
21
20
19
18
2
1
0
-1
-2
-3
-4
-5
-6
-7
-8
0.8
0.7
0.6
0.5
0.4
0.3
0.2
0.1
0
-0.1
-0.2
1985
1990
1995
AVHRR
STORM

Figure 4

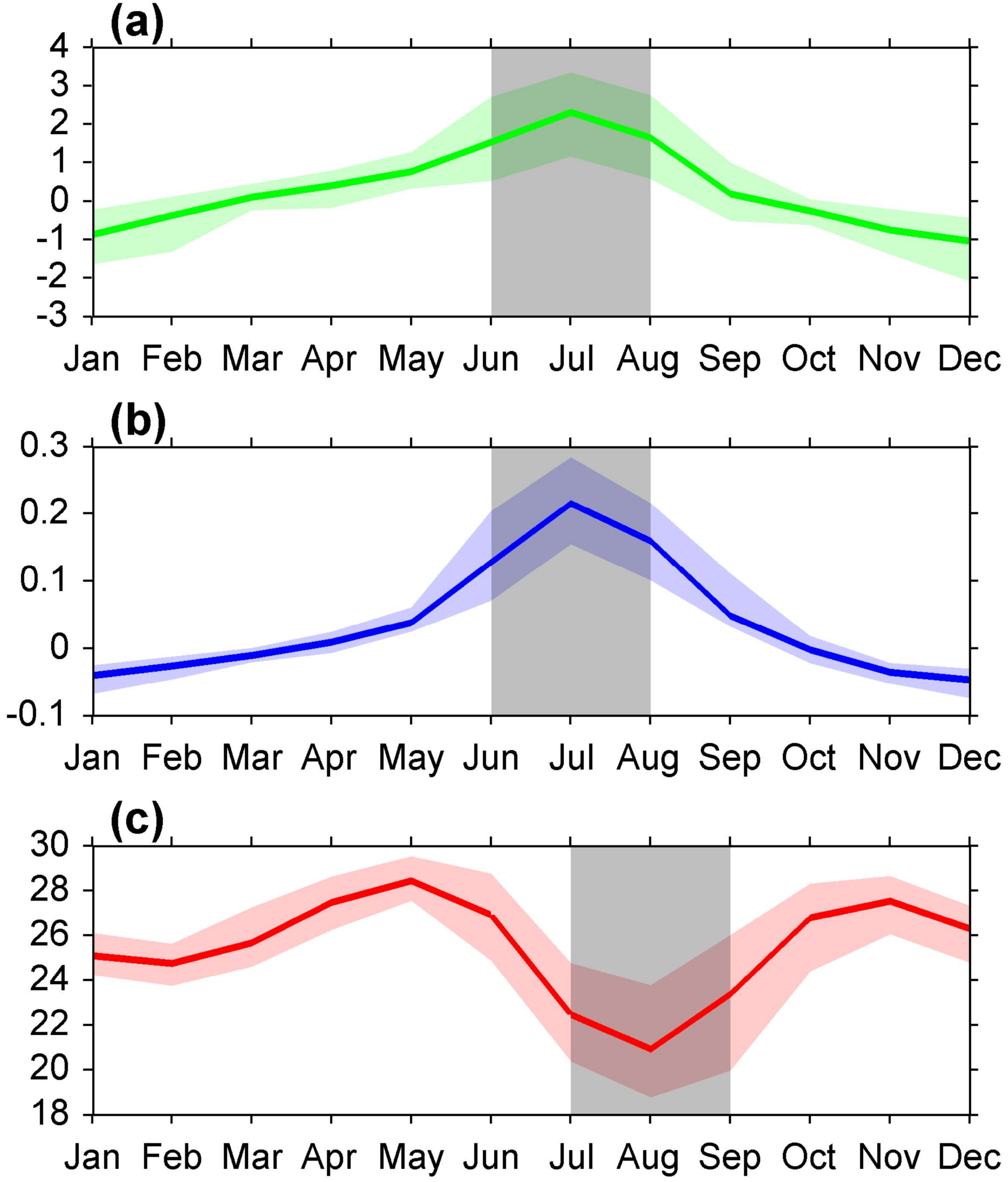

(a)
4
3
2
1
0
-1
-2
-3
Jan Feb Mar Apr May Jun Jul Aug Sep Oct Nov Dec
(b)
0.3
0.2
0.1
0
-0.1
Jan Feb Mar Apr May Jun Jul Aug Sep Oct Nov Dec
(c)
30
28
26
24
22
20
18
Jan Feb Mar Apr May Jun Jul Aug Sep Oct Nov Dec

Figure 5

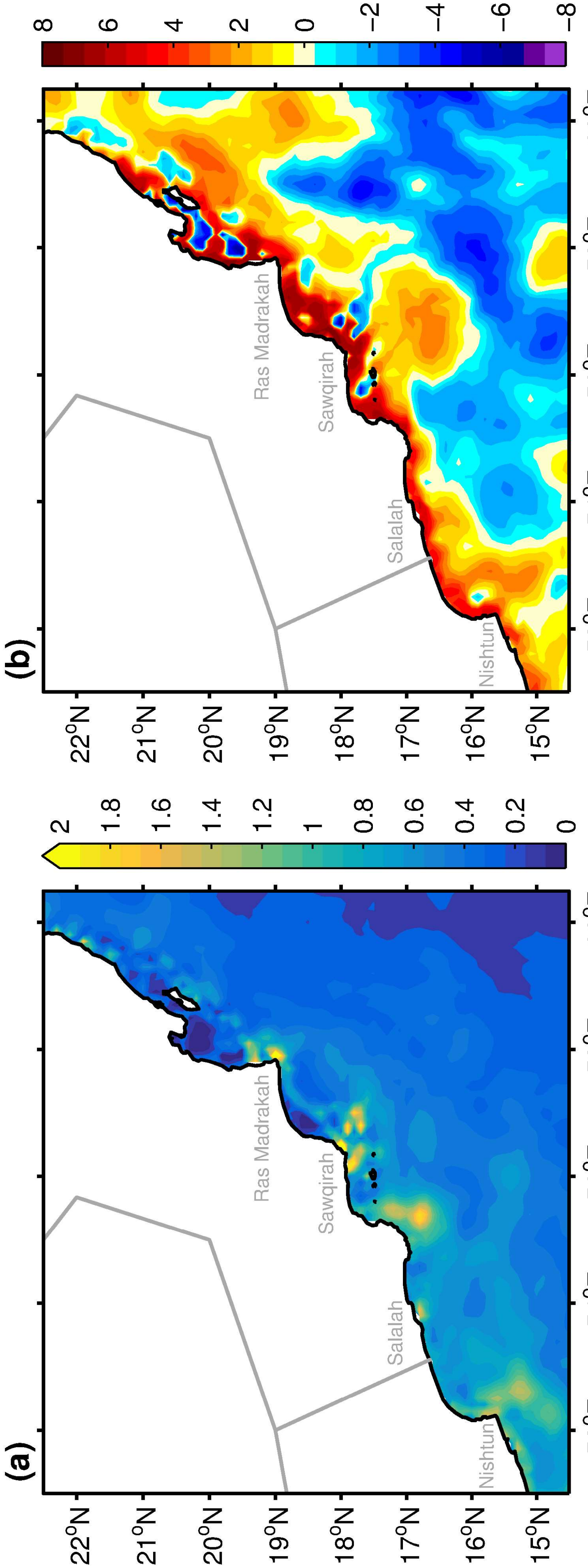

(a)
(b)
Ras Madrakah
Sawqirah
Salalah
Nishtun
22°N
21°N
20°N
19°N
18°N
17°N
16°N
15°N
52°E
54°E
56°E
58°E
60°E
2
1.8
1.6
1.4
1.2
1
0.8
0.6
0.4
0.2
0
8
6
4
2
0
−2
−4
−6
−8

Figure 6

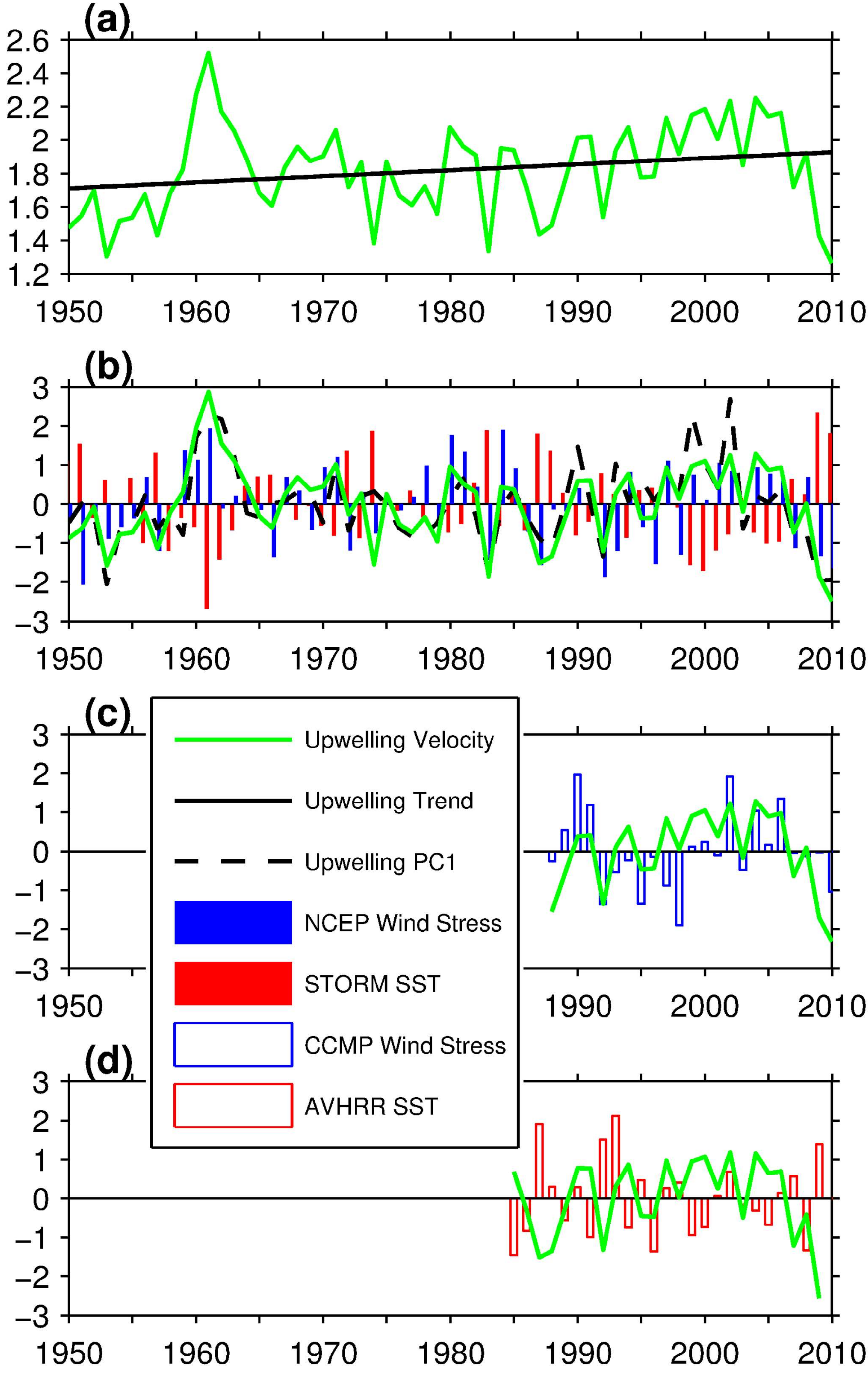

(a)
2.6
2.4
2.2
2
1.8
1.6
1.4
1.2
1950
1960
1970
1980
1990
2000
2010
(b)
3
2
1
0
−1
−2
−3
(c)
(d)
Upwelling Velocity
Upwelling Trend
Upwelling PC1
NCEP Wind Stress
STORM SST
CCMP Wind Stress
AVHRR SST

Figure 7

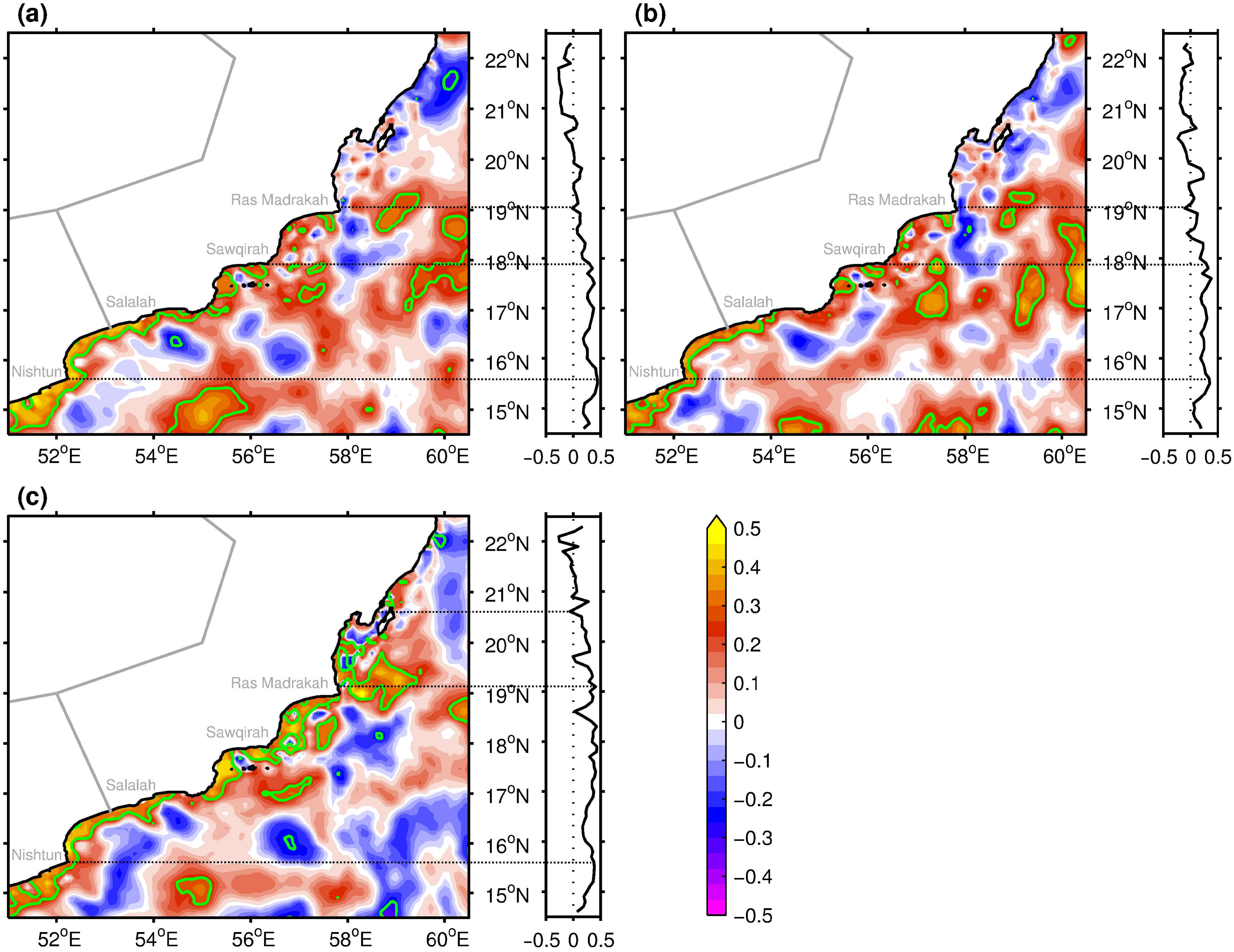

(a)
(b)
(c)
Ras Madrakah
Sawqirah
Salalah
Nishtun
52°E
54°E
56°E
58°E
60°E
22°N
21°N
20°N
19°N
18°N
17°N
16°N
15°N
−0.5 0 0.5
0.5
0.4
0.3
0.2
0.1
0
−0.1
−0.2
−0.3
−0.4
−0.5

Figure 8

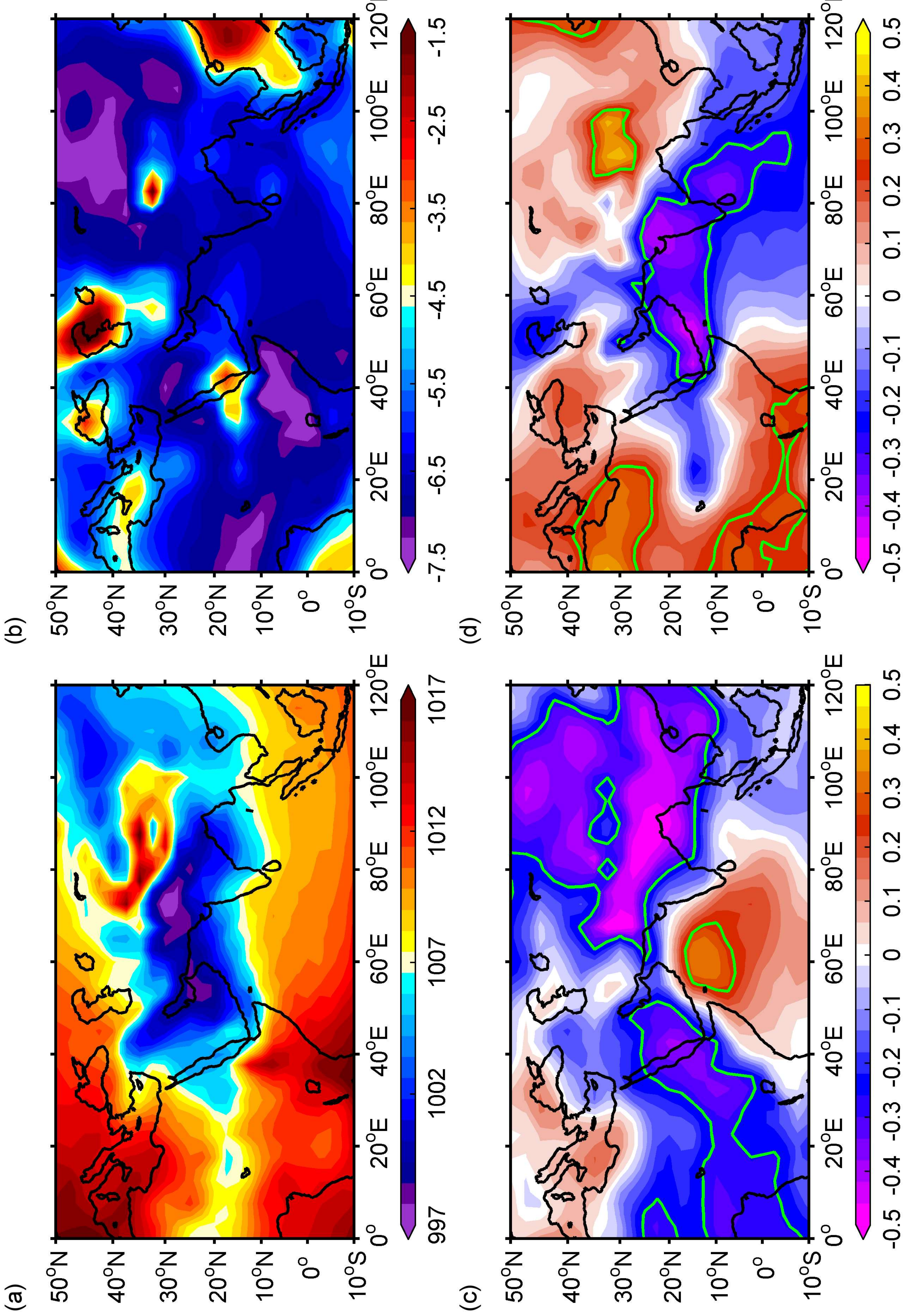

(a)
(b)
(c)
(d)
50°N
40°N
30°N
20°N
10°N
0°
10°S
0°
20°E
40°E
60°E
80°E
100°E
120°E
997
1002
1007
1012
1017
-7.5
-6.5
-5.5
-4.5
-3.5
-2.5
-1.5
-0.5 -0.4 -0.3 -0.2 -0.1 0 0.1 0.2 0.3 0.4 0.5

Figure 9

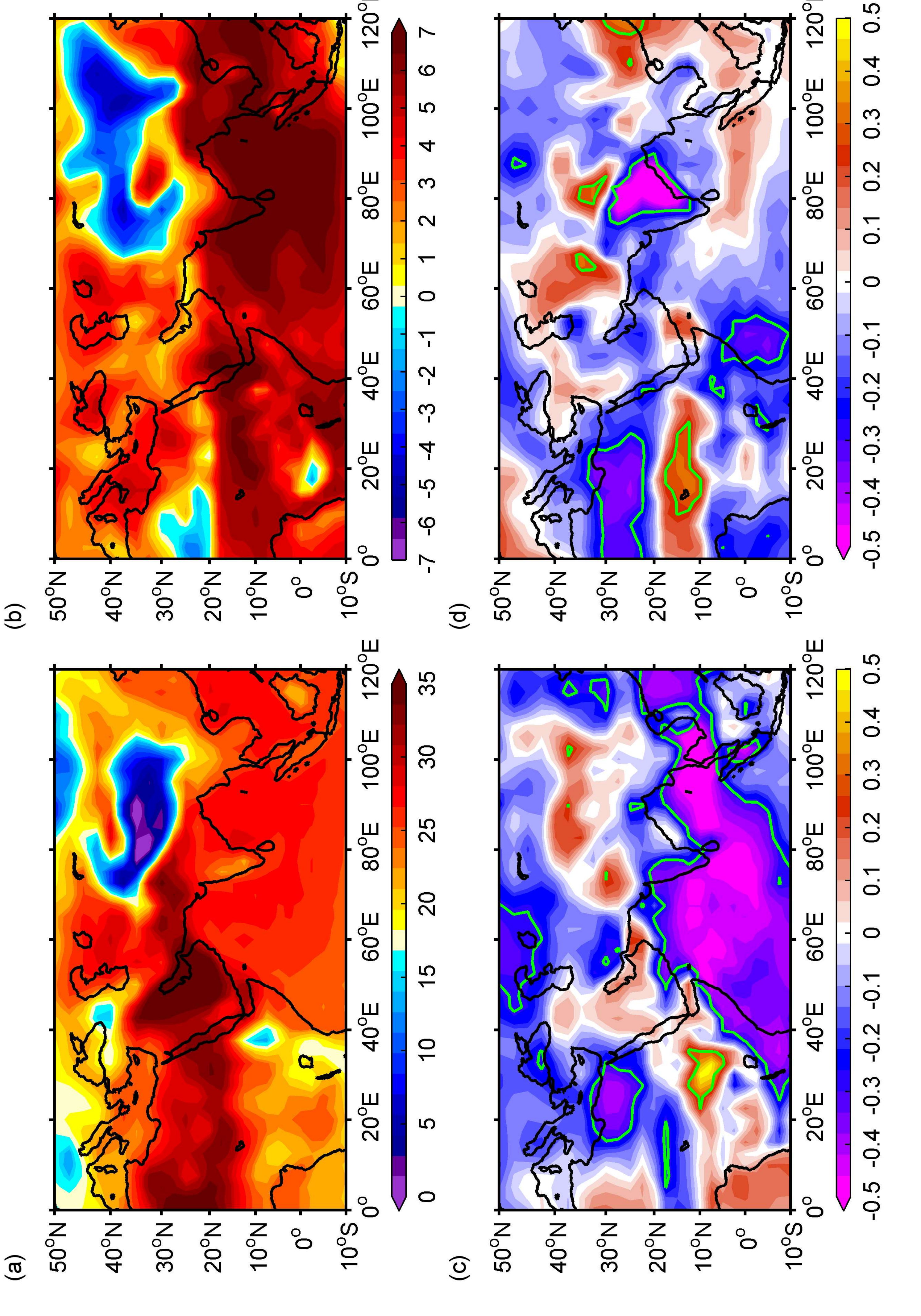

(a)
(b)
(c)
(d)
50°N
40°N
30°N
20°N
10°N
0°
10°S
0°
20°E
40°E
60°E
80°E
100°E
120°E
0
5
10
15
20
25
30
35
-7
-6
-5
-4
-3
-2
-1
0
1
2
3
4
5
6
7
-0.5
-0.4
-0.3
-0.2
-0.1
0
0.1
0.2
0.3
0.4
0.5